Basicity of N5 in semiquinone enhances the rate of respiratory electron outflow in *Shewanella oneidensis* MR-1

Yoshihide Tokunou[1,2], Keisuke Saito[1,3], Ryo Hasegawa[1], Kenneth H. Nealson[4], Kazuhito Hashimoto[2], Hiroshi Ishikita[1,3], and Akihiro Okamoto[2,5]*

*To whom correspondence should be addressed.
E-mail: OKAMOTO.Akihiro@nims.go.jp
Tel: +81-29-860-4430

Affiliations:
1. Department of Applied Chemistry, The University of Tokyo, 7-3-1 Hongo, Bunkyo-ku, Tokyo 113-8656, Japan.
2. International Center for Materials Nanoarchitectonics, National Institute for Materials Science, 1-1 Namiki, Tsukuba, Ibaraki 305-0044, Japan.
3. Research Center for Advanced Science and Technology, The University of Tokyo, 4-6-1 Komaba, Meguro-ku, Tokyo 153-8904, Japan.
4. Department of Earth Sciences, University of Southern California, Los Angeles, CA 90089, USA.
5. Center for Functional Sensor & Actuator, National Institute for Materials Science, 1-1 Namiki, Tsukuba, Ibaraki 305-0044, Japan

Abstract

Extracellular electron transport (EET) occurs in environmental iron-reducing bacteria and is mediated by an outer membrane multi-heme cytochrome complex (Cyts). It has critical implications for global mineral cycling and electrochemical microbial catalysis. The rate of EET mediated by multiple heme redox centers significantly increases in the presence of flavins and quinones. Their electron free energy does not entirely account for the fact that differential effects on EET rate enhancement vary significantly by factors ≥100. Here, we report on whole-cell electrochemical analysis of *Shewanella oneidensis* MR-1 using six flavin analogs and four quinones. We demonstrated that protonation of the nitrogen atom at position 5 (N5) of the isoalloxazine ring is essential for electron outflow acceleration as a bound non-covalent cofactor of Cyts. EET mediated by Cyts was accelerated at a rate dependent on pK_a(N5). The EET rate largely decreased in response to the addition of deuterated water (D_2O), while low concentration of D_2O (4 %) had little impact on electron free energy difference of the heme and non-covalent bound cofactors, strongly suggesting that the protonation of N5 limits the rate of EET. Our findings directly link EET kinetics to proton transport reaction via N5 and provide a basis for the development of novel strategies for controlling EET-associated biological reactions.

Keywords: Extracellular electron transport; Flavin; Kinetic isotope effect; Proton transfer; Whole-cell electrochemistry

42 **Significance statement**

43 The potential of various small molecules such as flavins and quinones to enhance the rate of
44 extracellular electron transport (EET) has been exploited to develop environmental energy
45 conversion systems. Flavins and quinones have similar molecular structures but their abilities
46 to enhance EET vary by >100× in *Shewanella oneidensis* MR-1. These large differences are
47 inconsistent with conventional models, which rely on redox potentials or diffusion constant of
48 shuttling electron mediators. In this study, we demonstrated that the basicity of the nitrogen
49 atom of the isoalloxazine ring (N5) enhances the rate of electron outflow when a flavin or
50 quinone is a non-covalent cofactor of *S. oneidensis* MR-1 outer membrane *c*-type
51 cytochromes.
52

Introduction

Extracellular electron transport (EET) is the process through which prokaryotes move electrons between the membrane interior and the cell exterior, such that redox reactions can occur with otherwise unavailable extracellular electron donors or acceptors (1-4). Microbes with the EET molecular machinery can render innovative metabolic processes inaccessible to microbes without the EET machinery. These include redox reactions with solid minerals (1, 2), intercellular electron transfer (5, 6), and surface interactions with electrodes for application in energy production and environmental technologies (7-11). The role of redox molecules as enhancers of bacterial current production remains controversial. High exogenous quinone concentrations (≥10 μM) enhance EET via an electron-shuttling mechanism, which is a two-electron redox process (12-14). In contrast, low levels of endogenous riboflavin or flavin mononucleotide (FMN) (≤1 μM) accumulate in cultures of EET-capable bacteria, non-covalently bind specific sites of outer membrane *c*-type cytochromes (Cyts) as cofactors (15-18), and form singly reduced semiquinone (SQ). Upon one-electron reduction of flavin, protonation occurs at the N5 nitrogen with the pK_a value (pK_a(N5)) of 8.6 (19).

SQ enhances the EET rate to the same extent as exogenous quinone-mediated shuttling despite hundredfold lower endogenous concentrations (15, 18, 20-23). Nevertheless, electron transfer mediated by SQ are thermodynamically unfavorable. The redox potentials (E_0) of the hemes in Cyts vary widely depending on the surrounding environment and are typically in the range of −400 to +200 mV relative to a standard hydrogen electrode (SHE) (24-32). SQ-mediated EET acceleration occurs when E_0 for Cyts is >+50 mV (vs. SHE) (15, 18, 20). SQ and oxidized flavin cycling have E_0 of ~ −100 mV (vs. SHE), which is >150 mV lower than those of the Cyt heme groups (15, 18, 20). Therefore, thermodynamically unfavorable electron transfer from Cyts to SQ is unlikely to enhance the EET rate. Bound and free flavins are crucial in numerous anaerobic electron bifurcation reactions using them as SQ intermediates (33, 34). Flavin-based EET functions as a major metabolic pathway in various Gram-positive bacteria such as the pathogen *Listeria monocytogenes* (35, 36) and in other metal reducing bacteria *Geobacter sulfurreducens* PCA (16).

The interactions of flavins with purified Cyts have been extensively investigated in the model EET-capable bacterium *Shewanella oneidensis* MR-1 (17, 37-40). On the other hand, stabilization of the SQ state in Cyts was confirmed only in intact cells (15, 20) possibly because of the structural complexity and dynamics of Cyt (41-44). Whole-cell approaches significantly limit access to molecular-level information about specific enzymes. Consequently, SQ-mediated EET rate enhancement mechanisms are unknown. Recently, a whole-cell electrochemical assay demonstrated that molecules analogous to riboflavin can

88 associate with Cyts in their single-electron reduced state (22). Thus, there is a potential
89 control mechanism for the interaction between the Cyts binding site and the SQ cofactor.
90 In the present study, we analyzed the influence of (i) various flavin analogs and
91 quinones on EET rate enhancement with respect to the pK_a of the flavin isoalloxazine ring;
92 (ii) pH on the E_0 for flavins and flavin analogs; and (iii) the kinetic isotope effect (KIE) on
93 EET with heavy water using intact *S. oneidensis* MR-1 cells. These data indicate that the
94 nitrogen atom at position-5 (N5) of the isoalloxazine ring determines the ability of the flavin
95 analog to bind Cyts and forms a semi-reduced (SR) intermediate analogous to SQ before
96 rapid and direct single-electron transfer. The protonation probability of N5 (i.e., pK_a(N5)) is
97 most likely a key determinant of the kinetic properties of EET.

Results and discussion

To identify the key properties of the flavin analogs and quinones involved in EET kinetics, we measured the rate and amount of current produced by *S. oneidensis* MR-1 during lactate oxidation (i_c) in the presence of riboflavin, flavin mononucleotide (FMN), six flavin analogs, and four quinones (Fig. 1A). We measured the formation of the semi-reduced (SR) state during i_c generation with each flavin and quinone using a three-electrode electrochemical system equipped with an indium tin-doped oxide (ITO) working electrode under +0.4 V (vs. SHE). Lactate (10 mM) served as the sole electron donor. Unless otherwise noted, the concentration of all flavin analogs and quinones tested was 2.0 μM. At this concentration, riboflavin strongly enhances i_c in *S. oneidensis* MR-1 as a bound cofactor by forming the intermediate SR state (15, 20). Flavin analogs with N5 in their polycyclic backbones (Fig. 1A) enhanced i_c at a rate equal to, or higher than that measured with riboflavin (Figs. 1B and S1A). MB gave the highest enhancement among N5 molecules. The dramatic i_c enhancement induced by MB was impaired by >90% via the deletion of the genes corresponding to Cyts (Fig. S1E). Similar substantial current decreases were also observed with riboflavin and FMN (15, 20). These data suggest that the N5-containing molecules enhance the rate of EET through Cyts, and their interactions with outer-membrane make negligible contributions to i_c as observed in several redox molecules (45, 46).

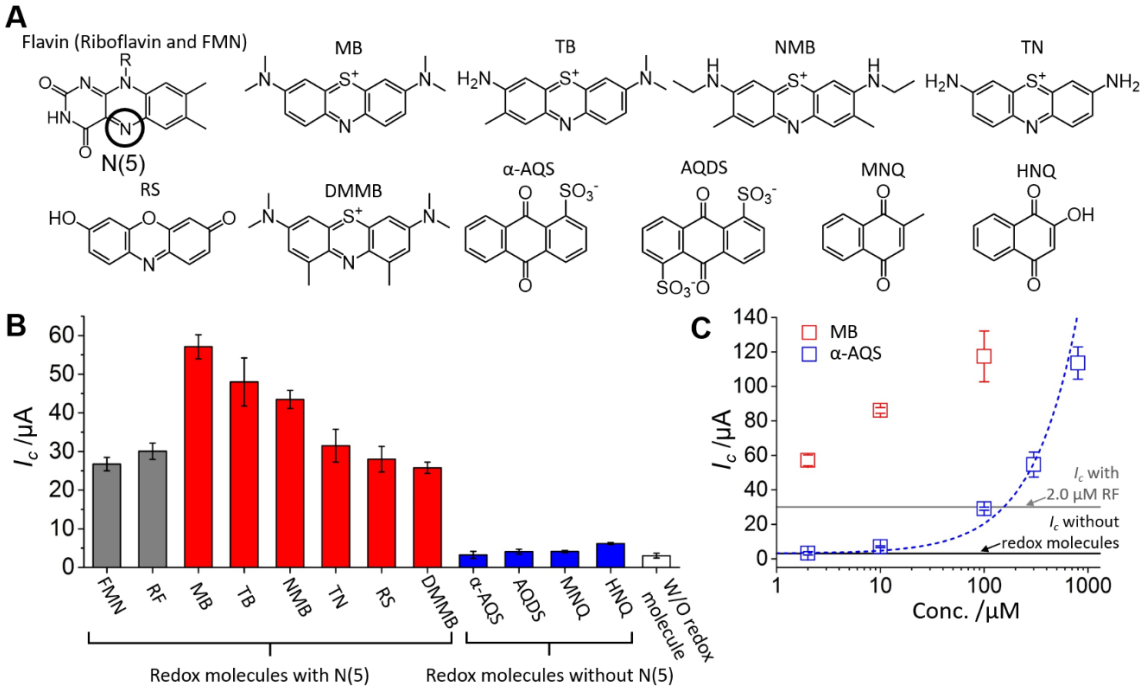

Fig. 1. (A) Chemical structures of the redox molecules used in the present study. N5 in the isoalloxazine ring is circled in the chemical structure of flavin. Methylene blue (MB),

toluidine blue (TB), new methylene blue (NMB), thionine (TN), resorufin (RS), and 1,9-dimethyl-methylene blue (DMMB) have N5, while anthraquinone-1-sulfonate (α-AQS), anthraquinone-1,5-disulfonate (AQDS), 2-methyl-1,4-naphthoquinone (MNQ), and 2-hydroxy-1,4-naphthoquinone (HNQ) lack it. (B) Maximum catalytic current of microbial lactate oxidation in *S. oneidensis* MR-1 (I_c) after 10 h measurement in the presence of each molecule shown in (A). I_c in the presence of flavin, flavin analogs, and quinones are represented as gray, red, and blue bars, respectively. Concentration of each redox molecule was set to 2.0 μM. Error bars represent mean ± SEM for ≥three individual experiments in separate reactors. (C) I_c vs. MB or α-AQS concentration in the reactor. Blue dotted line represents I_c estimated by Fick's law according to the diffusion kinetics of α-AQS between the cell and the electrode. Error bars represent the mean ± SEM for ≥three individual experiments in separate reactors.

Comparatively less EET enhancement was observed in the presence of quinones lacking N5 (blue bars in Figs. 1B and S1B). We compared the concentration dependencies of MB (with N5) and α-AQS (without N5) over 10 h using the max i_c value (I_c). I_c increased with α-AQS concentration in accordance with the α-AQS diffusion kinetics estimated by Fick's law (Figs. 1C and S1C). A concentration of 100 μM α-AQS was required to reach the same level of i_c as that achieved using 2.0 μM riboflavin, which is characteristic of diffusion-based shuttling mechanisms (Fig. 1C). The diffusion-limited kinetics of electron transfer from α-AQS to the electrode was previously confirmed by voltammetric analysis at scan rates of 1–100 mVs^{-1} in the presence of the *S. oneidensis* MR-1 biofilm (47). With an N5-containing molecule (N5 molecule), MB, I_c enhancement did not follow Fick's law and occurred at low concentrations (Fig. 1C and S1D). The observed scan rate dependency in cyclic voltammetry analysis indicated that the rate of electron transfer is not limited by diffusion kinetics in MB or riboflavin (Fig. S2). However, their kinetics were limited by diffusion in the absence of *S. oneidensis* MR-1 (Fig. S2). These data show that N5 molecules did not enhance i_c by a shuttling mechanism but rather by a direct electron transport process at the cell/electrode interface.

Stabilization of the N5 molecules in their SR form in Cyts was confirmed by the number of electrons involved in the redox reactions of all N5 molecules via differential pulse voltammetry (DPV) estimated from the half-width ($\Delta E_{p/2}$) of the oxidation peak (48, 49) (Figs. S3 and S4). Unbound MB in a cell-free system showed a $\Delta E_{p/2}$ of 55 mV which indicates a two-electron redox reaction (Fig. S3) (48, 49). The presence of *S. oneidensis* MR-1 cells changed the $\Delta E_{p/2}$ of MB to 120 mV (Fig. S3). This value resembles that reported for the one-

electron redox reaction of flavin bound with Cyts (130 mV) (15, 20). Therefore, MB is stabilized in its SR form in the presence of MR-1. The peak MB current decreased upon the addition of the free radical scavenger α-tocopherol (Fig. S5), which supports the formation of SR state (15, 50). The oxidative signal of MB showed a single peak corresponding to the SR state up to a concentration of 10 μM (Fig. S6). Thereafter, the increase of MB concentration gradually shifted the peak potential (E_p) towards the E_p of oxidation peak in two-electron reaction (Fig. S7). Therefore, MB would serve as a bound cofactor below 10 μM concentration in our experimental setup. In contrast, a one-electron oxidation peak was not detected for α-AQS (without N5) in the DP voltammogram (Fig. S8). These data demonstrate that MB enhances the rate of EET in the SR state. The same trend for $\Delta E_{p/2}$ was observed with TB, NMB, TN, RS, and DMMB (Fig. S4). These results suggest that the N5 atom in the polycyclic backbone is the critical structural component of flavin analogs, which enables them to function in the SR state as bound cofactors in Cyts. The formation of the SR state with electron flow enhancement is reminiscent of the SQ states observed in numerous microbial electron bifurcation reactions (33). Some of these have been confirmed in the crystal structures of flavodoxins in the oxidized quinone, semiquinone, and hydroquinone forms (51). It seems possible that the SR state is stabilized by donation of a hydrogen bond to N5 from the Cyts scaffold, as observed in flavodoxins (52).

To confirm whether the redox cycle of bound cofactors could couple with protonation as with that of SQ in flavodoxins, we evaluated the effects of bulk solution pH on the redox potential (E_0) using the oxidation peaks in DP voltammograms. When a bulk solution was acidified in the presence of *S. oneidensis* MR-1 and each cofactor at 2 μM, the E_0 of the N5 molecules, including riboflavin, linearly decreased upon pH increase, which indicates a proton-coupled electron transfer reaction (Fig. 2). On the other hand, the observed slope values were lower than expected (riboflavin: -13 mV pH^{-1}; MB: –34 mV pH^{-1}; TB: –32 mV pH^{-1}; NMB: –30 mV pH^{-1}; and TN: –21 mV pH^{-1} (Fig. 2)). Similar deviations from the -59 mV pH^{-1} slope were reported for SQs in certain flavodoxins and flavoproteins forming hydrogen bonds with protein scaffolds via N5 (53-55). The absence of the corresponding deviation in the free state flavins and quinones (53, 55) suggests that the low pH-dependence of E_0 could be due to conformational changes of the protein structure, which originates from changes of the protonation states of the titratable sites.

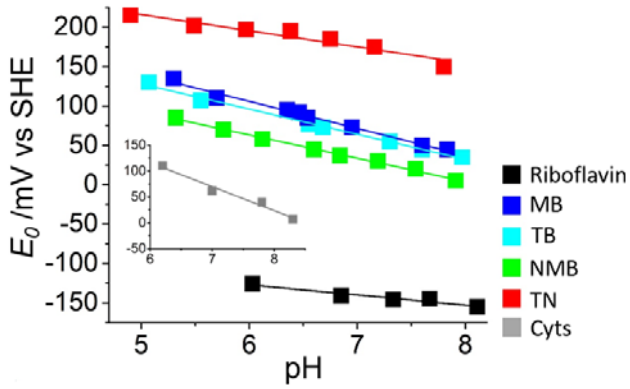

Fig. 2. E_0 of the bound cofactors (riboflavin, MB, TB, NMB, and TN) determined by DPV as a function of bulk solution pH. The slopes for the plots are riboflavin: -13 mV pH^{-1}; MB: -34 mV pH^{-1}; TB: -32 mV pH^{-1}; NMB: -30 mV pH^{-1}; and TN: -21 mV pH^{-1}. Inset: E_0 of Cyts derived from the DPV of riboflavin-bound Cyts. The slope was -47 mV pH^{-1} which is near the reported value for MtrC, a subunit of Cyts (56).

Given that the flavins receive electrons from the heme group(s) of Cyts, we previously posited that molecules with higher E_0 could be more favorable for the acceleration of EET in our condition (+0.4 vs. SHE) (15, 32). It is evident from Fig. 1B that the extent of EET rate enhancement varies depending upon the binding N5 molecules. Unexpectedly, the EET rate did not increase with higher E_0 in some N5 molecules (Fig. 3A). We approximated the capability of EET from the max i_c value (I_c) in the 10-h measurements of each of the N5 molecules at the concentration of the Cyts complex with bound cofactors (Fig. S9 and Table S1). Their E_0 were estimated by DPV (Figs. S3 and S4). It was assumed that the N5 molecules act as bound cofactors up to a concentration of 10 µM because of the DPV data (Figs. S6 and S7), and the EET capability for each Cyts forming a complex with bound cofactor was estimated from the dissociation constant (K_d) at the N5 molecule concentrations of 2–10 µM (Fig. S9). As shown in Fig. 3A, the EET rate increased with E_0 for the N5 molecules <+50 mV (vs. SHE). However, this tendency does not hold true for N5 molecules with higher E_0. The EET rate for RS was low possibly due to a low overpotential to be oxidized by the electrode. Nevertheless, the cutoff was nearly identical to E_0 for Cyts (+50 mV vs. SHE) (15, 32). The N5 molecules with E_0 >+50 mV accept electrons from Cyts in a thermodynamically favorable downhill reaction. Thus, the suppression of EET rate could not originate from energetics of electron transfer.

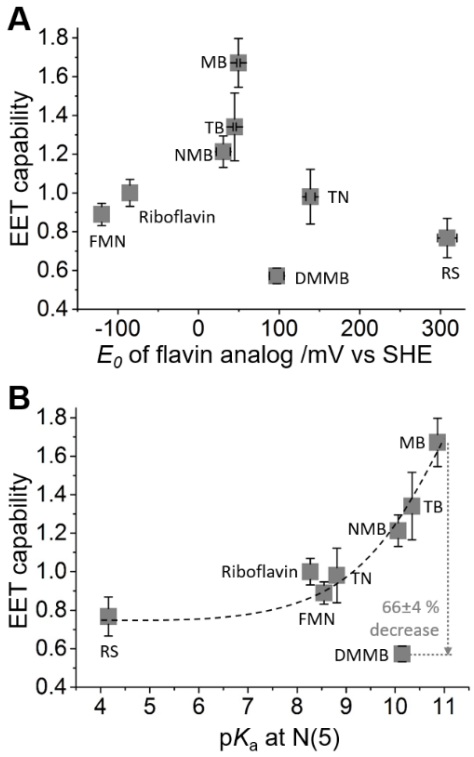

Fig. 3. EET capabilities of *S. oneidensis* MR-1 with each N5 molecule as a function of the E_0 of each cofactor (A) and pK_a(N5) in one-electron reduced form (B). The E_0 for all cofactors bound to Cyts except FMN and riboflavin were determined by differential pulse voltammetry (DPV) (Figs. S3 and S4). The E_0 for FMN and riboflavin were obtained from the literature (15, 20). The pK_a(N5) were calculated using a quantum chemical approach (Figs. S10 and S11). pK_a(N5) of FMN and riboflavin were obtained from the literature (19). Error bars represent the mean ± SEM for ≥three individual experiments. The gray dotted line shows the suppression of the EET capability of DMMB relative to MB. The dashed line is for visual guidance and orientation.

We compared pK_a(N5) with the EET capability of each N5 molecule. pK_a(N5) in the SR state was calculated using a quantum chemical approach, as demonstrated for 28 reference compounds (Figs. S10 and S11) (57, 58). EET capability increased with pK_a(N5) in the SR form (Fig. 3B). The increase in current production at high pK_a(N5) suggests that the N5 protonation of the singly reduced cofactor limits the rate of EET. Nucleophilicity at N5 was also estimated by the Hammett substituent parameters. EET capability increased with the increase of nucleophilicity at N5 (Fig. S12 and Table S2). Meanwhile, DMMB with pK_a of 10.14 showed ~66 ± 4% lower EET capability than MB (Fig 3B). Since DMMB has the identical backbone structure with MB except for methyl groups at the vicinity of N5 moiety in

the isoalloxazine ring, strict suppression of EET capability in DMMB may be caused by prevention of protonation at N5. In contrast, there was no clear relationship between current production and pK_a value in the two-electron reduced form (Fig. S13). In the electron-shuttling mechanism involving a two-electron redox process, the rate limiting factors for EET are the diffusion constant and the E_0 value (59). The distinct rate-limiting step from shuttling mechanism supports the bound-cofactor mechanism of the N5 molecules which mediate one-electron redox process as binding SR species, and supports the importance of proton uptake capability at N5 in EET kinetics.

To analyze the rate-limiting step in EET, we evaluated the kinetic isotope effect (KIE) using a highly reproducible *S. oneidensis* MR-1 monolayer biofilm (47, 60). We added deuterated water (≤ 4%; subtoxic concentration) to the bulk solution during current production of the MR-1 monolayer biofilm in the presence of 2.0 μM of each cofactor molecule. A previously reported experimental setup was used (47, 60). As the i_c was limited by the EET process, the KIE could characterize the rate-limiting proton transfer process through cofactor-bound Cyts (47). The influence of the KIE on the EET rate was evaluated from the differences in current production 10 min after D_2O and H_2O ($i_c(H_2O)/i_c(D_2O)$) were added to the electrochemical system. The amount of cofactor-bound Cyts complex was normalized by a dissociation constant (K_d) in the presence and absence of 4% D_2O (Fig. S9). D_2O lowered current production within 10 s in the presence of TN (Fig. 4A). Further addition of D_2O up to a final concentration of 4% continued to reduce the current (Fig. 4C). In contrast, the current increased by D_2O addition in the presence of MB (Fig. 4B). The lower K_d value of MB was estimated in the presence of D_2O (Fig. S9), and it caused the higher i_c. The KIE for the cofactor-bound Cyts normalized to 1.06 ± 0.07, and those of riboflavin and TN were 1.35 ± 0.03 and 1.46 ± 0.10, respectively (Fig. 4D). These KIE values were larger than those measured in the presence of 100 μM α-AQS (gray dashed line in Fig. 4D), where the EET rate is limited by diffusion of α-AQS (47), strongly suggesting that the observed KIE values are assigned to riboflavin- and TN-bound Cyts. Therefore, the KIE data indicate that the EET mediated by cofactor-bound Cyts is limited by proton transport process. Substantial differences in KIE were detected when the cofactors in the Cyts were replaced. Therefore, each cofactor has its own unique KIE, and each N5 protonation/deprotonation most likely limits the EET rate. This finding is consistent with a previous report which suggested an association of rate-limiting proton transport with electron transport in flavin-bound Cyts (47).

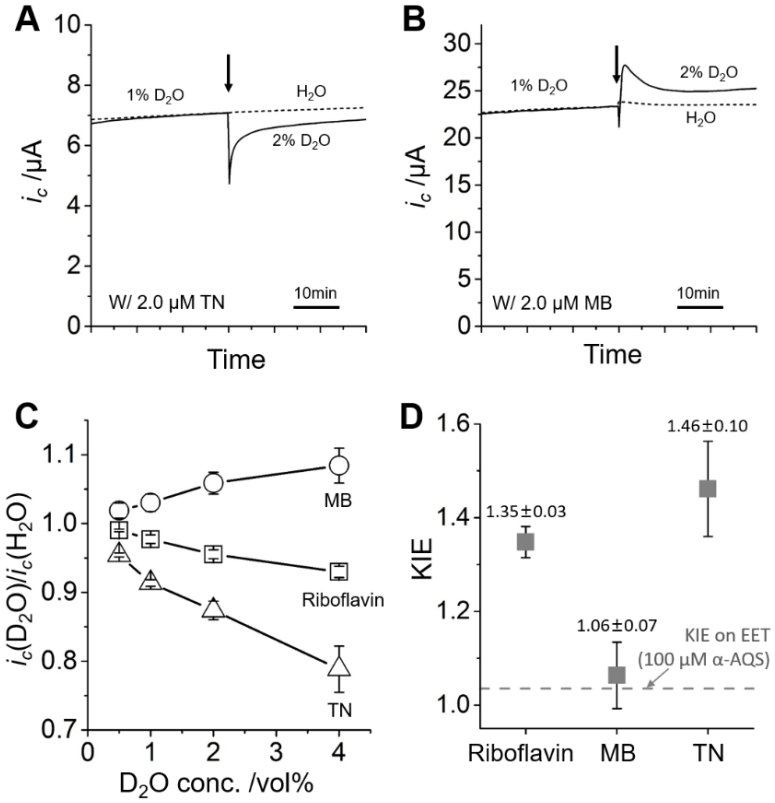

Fig. 4. Effect of deuterium ion on EET kinetics in the presence of redox molecules. Representative time course for current production in the *S. oneidensis* MR-1 monolayer biofilm in the presence of 2.0 μM TN (A) and MB (B). The arrows indicate the time points of D_2O (solid line) or H_2O (dotted line) addition. Data corresponding to the dotted line were normalized to the data point immediately before D_2O addition in the solid line data. (C) Effect of D_2O addition at subtoxic concentrations (≤ 4% v/v) on i_c in the presence of 2.0 μM MB (circle plots) or TN (triangle plots). Data for 2.0 μM riboflavin (square plots) were obtained from the literature (47) for comparison. Error bars represent the mean ± SEM for ≥three experiments in separate reactors. (D) Kinetic isotope effect (KIE) on the EET per unit concentration of the cofactor-bound Cyts complexes in 4% (v/v) D_2O. Error bars represent mean ± SEM for ≥three experiments in separate reactors. Gray dashed line represents the KIE on EET for 4% (v/v) D_2O in the presence of 100 μM α-AQS reported in ref. (47). Numeric data are indicated above each plot.

The rate-limiting proton transfer is associated with the electron transfer from the hemes in the Cyts to the bound cofactors, and E_0 potentially affect the EET rate (Fig. 3A). Consequently, any alteration in the E_0 gap between Cyts and bound cofactors may increase the KIE values. To confirm that the observed KIE values were derived substantially from

rate-limiting proton transfer rather than any change in E_0 in the presence of D_2O, we evaluated the E_p of Cyts, riboflavin, TN, and MB after D_2O addition. Fig. 5 shows representative oxidation peaks obtained from the DP voltammograms of *S. oneidensis* MR-1 monolayer biofilm in the presence of 2.0 μM riboflavin, TN, or MB before and after the addition of 4% D_2O. To determine E_p values, subtraction and deconvolution were conducted using an open source program SOAS (61). In D_2O, not only a positive shift in the E_p of ~25 mV for hemes in the Cyts but also a positive shift in the E_p of ~25 mV for bound riboflavin were observed, without changing the E_p difference (Fig. 5A). The E_p for TN also positively shifted, and the E_p gap between Cyts and TN was also almost identical (Fig. 5B). Peaks of Cyts and MB were overlapped in both before and after addition of D_2O (Fig. 5C), indicating little impact of D_2O on E_p gap as well. Decrease of peak width in the presence of D_2O may originate from the increase of MB/Cyts ratio contributing on the oxidation peak, which is consistent with higher affinity of MB with Cyts in the presence of D_2O (Fig. S9). Collectively, E_p gap between Cyts and bound cofactors were scarcely influenced by D_2O, further supporting that the observed KIE values in Fig. 4 were derived substantially from rate-limiting proton transfer via N5 of the bound cofactors.

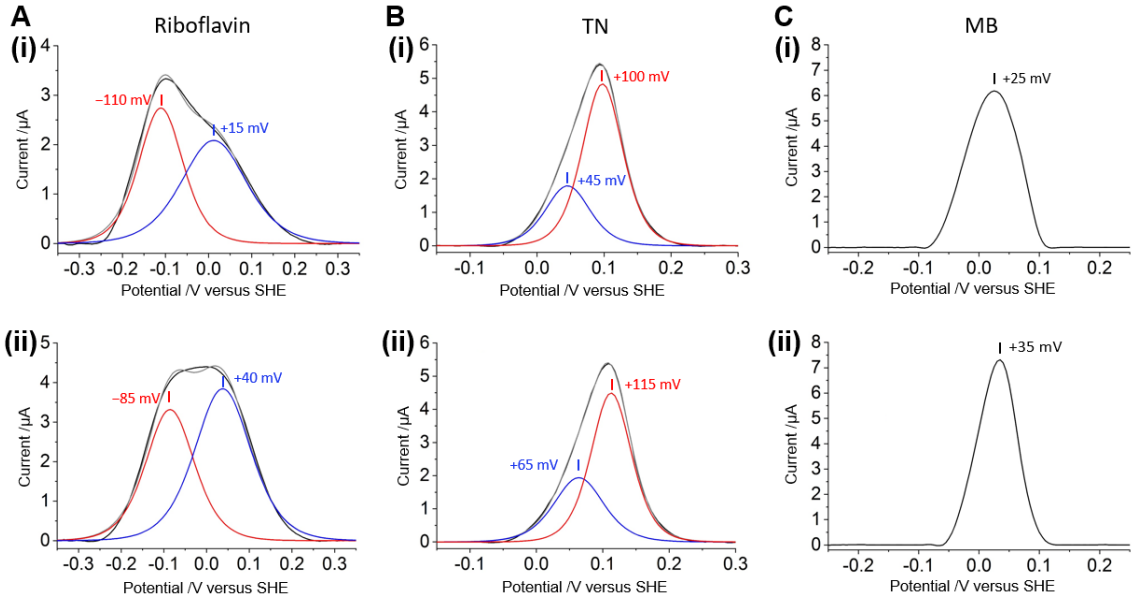

Fig. 5. Baseline subtracted differential pulse (DP) voltammograms of the *S. oneidensis* MR-1 monolayer biofilm in the presence of 2.0 μM riboflavin (A), TN (B), and MB (C). (i) and (ii) represent the data before and after the addition of 4% (v/v) deuterium oxide, respectively. Black and gray lines are baseline subtracted DP voltammograms and fitted lines, respectively. Red and blue lines represent oxidation peaks deconvoluted from fitted line. According to (15, 20), the blue peak is assigned to the Cyts and the red peak is assigned to a bound cofactor.

The oxidative peaks in panel (C) were not able to be deconvoluted by SOAS because they overlapped.

The extent of current suppression by deuterated water was much larger than those determined when the EET kinetics is limited by diffusion process of proton donor for N5 (Fig. 4D). Assuming protons are delivered to N5 via diffusing water or buffer molecules in bulk solution and it limits the rate of EET, the ratio of the cofactor proceeding EET with D^+/H^+ is correlated with the percentage of heavy water added, i.e., the extent of current suppression is lower than the percentage of deuterated water added (62, 63). However, we observed the KIE values >1.04 in the presence of 4% D_2O (Fig. 4D), indicating that diffusion of free water or buffer molecule do not limit the rate of EET. Some enzymes with several protonic sites transporting more than one proton suppress the rate of coupled electron transport over the ratio of added deuterated water as indicated in the Gross-Butler model (62, 64, 65). Given such protonation kinetics is not possible for free flavin or quinone, the observed large KIE further confirms our finding that the protonation of bound-cofactor limits the rate of EET via Cyts.

The EET kinetics through Cyts was reported to be limited by proton transfer reaction in the absence of SR cofactor molecules (47). Therefore, high EET acceleration by cofactors may be the result of an increase in the rate of proton transfer coupled with the EET. Given EET links with the localization of protons across the inner-membrane as well in the absence of the bound cofactors (47, 66), it is of great interest to clarify detailed molecular mechanisms of EET-coupled complex proton transport to understand energy acquisition machinery of EET-capable bacteria in the presence and absence of the bound cofactors.

Conclusions

We demonstrated that the basicity of N5 enhances the rate of EET when flavin is stabilized as SQ in Cyts of *S. oneidensis* MR-1. Therefore, high EET acceleration by the SQ intermediate in spite of unfavorable electron energetics may result from enhancement of proton transfer rate coupled with the EET. Significant variations in EET enhancement caused by flavin analogs and quinones are also explained by the function of N5, the proton uptake capability and the ability to form SR state binding with Cyts (Fig. 6). It is of great interest to test the function of N5 with the EET-capable bacterium *Geobacter sulfurreducens* and the pathogen *Listeria monocytogene* which use bound-flavin based EET mechanism as well (16, 35, 36). Understanding the role of the N5 and SR state associated with EET may help elucidate the function of redox bifurcation in biological systems, and could provide novel direction to control environmental and pathogenic bacterial activity.

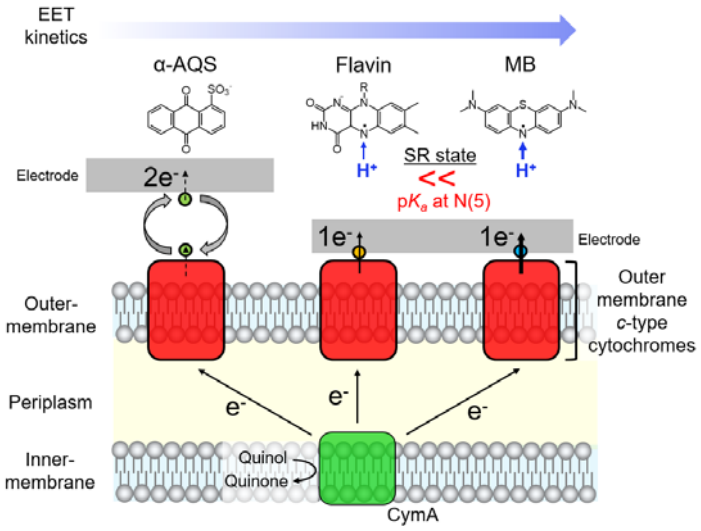

Fig. 6. Schematic representation of the molecular control of respiratory electron outflow in *S. oneidensis* MR-1 mediated by flavin, flavin analogs, and quinones.

Methods

Strains and culture conditions

Shewanella oneidensis MR-1 cells were grown aerobically at 30 °C for 24 h in 15 mL Luria-Bertani (LB) medium (25 g L^{-1}). The cell suspension was centrifuged at 6,000 × *g* for 10 min. The cell pellet was resuspended in 15 mL of a medium consisting of DM: $NaHCO_3$ [2.5 g L^{-1}], $CaCl_2 \cdot 2H_2O$ [0.08 g L^{-1}], NH_4Cl [1.0 g L^{-1}], $MgCl_2 \cdot 6H_2O$ [0.2 g L^{-1}], NaCl [10 g L^{-1}], yeast extract [0.5 g L^{-1}], and (2-[4-(2-hydroxyethyl)-1-piperazinyl] ethanesulfonic acid [HEPES; 7.2 g L^{-1}] (pH 7.8) supplemented with 10 mM lactate as the carbon source for *S. oneidensis* MR-1. The cells were cultured aerobically at 30 °C for 12 h and centrifuged at 6,000 × *g* for 10 min. The cell pellet was washed twice with DM medium by centrifugation for 10 min at 6,000 × *g*. A mutant strain lacking the genes encoding Cyts (Δ*omcAll*; deletions of *SO1778-SO1782*, *SO2931*, and *SO1659*) was constructed as previously described (67).

Electrochemical measurements of the catalytic current generated by lactate oxidation (i_c) in S. oneidensis *MR-1 with each redox molecule*

A single-chamber, three-electrode system for whole-cell electrochemistry was constructed as previously described (15, 22). An indium tin-doped oxide (ITO) substrate (surface area: 3.1 cm^2) was placed at the bottom of the reactor and used as the working electrode. Ag/AgCl (saturated KCl) and a platinum wire (surface area: ~10 mm^2) were used as the reference- and counter- electrodes, respectively. DM 4.0 mL (pH 7.8) containing each redox molecule (Fig. 1A) and 10 mM lactate as the sole electron donor was de-aerated by bubbling with N_2 for > 20 min. It was then added to the electrochemical cell as an electrolyte. The concentration of flavin analogs and quinones was set to 2.0 μM unless otherwise indicated. The reactor was maintained at a temperature of 30 °C and was not stirred during measurements. Cell suspensions with OD_{600} = 0.1 were inoculated into the reactor. The working electrode was poised at +0.4 V vs. the standard hydrogen electrode (SHE). Electrochemistry-based experimental details about estimation of dissociation constant (K_d), EET capability, and KIE value are described in Supporting information.

Formation of the S. oneidensis *MR-1 monolayer biofilm on the ITO electrode*

DM 4.0 mL (pH 7.8) with 10 mM lactate was added to the electrochemical cell as an electrolyte and was de-aerated by bubbling with N_2 for > 20 min. The *S. oneidensis* MR-1 cell suspension with OD_{600} = 0.1 was grown in the reactor. The working electrode was poised at +0.4 V vs. SHE in the presence of 10 mM lactate as the sole electron donor. The bacteria

were incubated at 30 °C with no agitation for 25 h. Formation of the monolayer biofilm was confirmed by *in situ* confocal fluorescence microscopy as previously described (32).

Voltammetry conditions

Cyclic voltammetry (CV) and differential pulse voltammetry (DPV) were conducted to determine the electrochemical properties of the flavin analogs and quinones and the *S. oneidensis* MR-1 monolayer biofilm via an automatic polarization system (VMP3; BioLogic Science Instruments, Seyssinet-Pariset, France). DPV was conducted under the following conditions: 5.0 mV pulse increments, 50 mV pulse amplitude (ΔE_{pa}), 300 ms pulse width, and 5.0 s pulse period. E_0 was approximated from the equation $E_0 = E_p + (\Delta E_{pa}/2)$ (48), thus, E_0 was estimated to be 25 mV more positive than the peak potential (E_p) observed in DPV. To determine the peak potential (E_p), half-width ($\Delta E_{p/2}$), and oxidation peak intensity in DPV, the background current was subtracted by fitting the baseline of regions remote from the peak and assuming a similar smooth charging current throughout the peak region. The subtraction was performed in the open source program SOAS (61).

Calculation of the acid-base equilibrium dissociation constants (pK_a) in redox active molecules.

To compute the absolute pK_a values, we employed a quantum chemical approach (57). In the deprotonation reaction of the protonated state (AH) to deprotonated state (A^-) in aqueous solution, pK_a is defined as

$$\mathrm{p}K_a = \frac{\Delta G_{aq}}{2.303\,RT} \qquad \text{(eq. 1)}$$

where ΔG_{aq} is the free energy difference between AH and (A^- + H^+) in water (i.e., $\Delta G_{aq} = G_{aq}(A^-) + G_{aq}(H^+) - G_{aq}(AH)$), R is the gas constant, and T is the temperature. ΔG_{aq} can also be written as

$$\Delta G_{aq} = \Delta G_{gas} + \Delta G_{solv}(A^-) + \Delta G_{solv}(H^+) - \Delta G_{solv}(HA) \qquad \text{(eq. 2)}$$

$$\Delta G_{gas} = G_{gas}(A^-) + G_{gas}(H^+) - G_{gas}(AH) \qquad \text{(eq. 3)}$$

The free energy G_{gas} in vacuum can be obtained, using the following equation;

$$G_{gas} = E_0 + ZPE + \Delta G_{0\rightarrow 298K} \qquad \text{(eq. 4)}$$

where E_0 is the ground-state energy in vacuum, ZPE is the zero-point vibrational energy, and $\Delta G_{0\rightarrow 298K}$ is the thermal vibrational free energy at 298 K. For proton, the free energy $G_{gas}(H^+)$ of 6.28 kcal/mol and $\Delta G_{solv}(H^+)$ of 265.74 kcal/mol were used (57). To obtain E_0, ZPE, and $\Delta G_{0\rightarrow 298K}$, full geometry optimizations were carried out using the restricted DFT method for

the non-radical states and the unrestricted DFT method for the radical states with the B3LYP functional and 6-31g** basis sets, and we used the Jaguar program code (68). Vibrational frequencies and electrostatic potentials were calculated using the geometry-optimized structures at the same level of theory. To calculate the ground-state electronic energy E_0, we employed cc-pvqz basis sets for accuracy.

The solvation energy ΔG_{solv} was calculated by solving the Poisson equation using the Solvate module from MEAD (69) , where van der Waals radii for H, N, O, Cl, and titratable H^+ are 1.2, 1.4, 1.4, 1.9, and 1.0 Å, respectively; C for $-CH_3$ and $-CH_2-$ groups are 2.0 Å, whereas C for others are 1.2 Å (57). Atomic partial charges used for ΔG_{solv} were determined by the restraint-electrostatic-potential (RESP) method (70-72).

To evaluate the accuracy of the method, we calculated pK_a values for 28 compounds whose experimentally measured pK_a values are reported (i.e., ref. (73) for H_2O and NH_4^+ and ref. (57) for other compounds) (Fig. S10B). We reproduced the experimentally measured pK_a values with a root-mean square deviation of 0.94 and a maximum error of 1.77 in pK_a units (Fig. S11).

Acknowledgements

The authors thank Prof. Hiroyuki Noji and Prof. Kohei Uosaki for their helpful advice. This work was financially supported by JST CREST (No. JPMJCR1656), JSPS KAKENHI (No. 24000010 to K.H., No. 17H04969 to A. O., No. 17J02602 to Y.T., No. JP26800224 to K.S., No. JP16H06560 to K.S and H.I., and No. JP26105012 to H.I.), the Japan Agency for Medical Research and Development (AMED), the US Office of Naval Research Global (No. N62909-17-1-2038), the Materials Integration for Engineering polymers of the Cross-ministerial Strategic Innovation Promotion Program (SIP), and the Interdisciplinary Computational Science Program in CCS, University of Tsukuba. Y.T. is a JSPS Research Fellow and supported by JSPS through the Program for Leading Graduate Schools (MERIT).

Author contributions

Y.T. and A.O. conceived and designed the study. Y.T. conducted the experiments and analyses. K.S., R.H., and H.I. conducted the theoretical calculations. Y.T., K.H.N., K.H., H.I., and A.O. wrote the manuscript.

Competing financial interests

The authors declare that there are no competing financial interests.

Materials & Correspondence

OKAMOTO.Akihiro@nims.go.jp

453 **References**

454

455 1. Lovley DR & Phillips EJ (1988) Novel mode of microbial energy metabolism: organic
456 carbon oxidation coupled to dissimilatory reduction of iron or manganese. *Appl.*
457 *Environ. Microbiol.* 54(6):1472-1480.
458 2. Myers CR & Nealson KH (1988) Bacterial Manganese Reduction and Growth with
459 Manganese Oxide as the Sole Electron-Acceptor. *Science* 240(4857):1319-1321.
460 3. Kim BH, Kim HJ, Hyun MS, & Park DH (1999) Direct electrode reaction of Fe(III)-
461 reducing bacterium, *Shewanella putrefaciens*. *J. Microbiol. Biotechnol.* 9(2):127-131.
462 4. Bond DR, Holmes DE, Tender LM, & Lovley DR (2002) Electrode-reducing
463 microorganisms that harvest energy from marine sediments. *Science* 295(5554):483-
464 485.
465 5. Summers ZM, *et al.* (2010) Direct Exchange of Electrons Within Aggregates of an
466 Evolved Syntrophic Coculture of Anaerobic Bacteria. *Science* 330(6009):1413-1415.
467 6. McGlynn SE, Chadwick GL, Kempes CP, & Orphan VJ (2015) Single cell activity
468 reveals direct electron transfer in methanotrophic consortia. *Nature* 526(7574):531-
469 535.
470 7. Logan BE, *et al.* (2006) Microbial fuel cells: Methodology and technology. *Environ.*
471 *Sci. Technol.* 40(17):5181-5192.
472 8. Busalmen JP, Esteve-Nunez A, Berna A, & Feliu JM (2008) *C*-type cytochromes wire
473 electricity-producing bacteria to electrodes. *Angew. Chem. Int. Ed.* 47(26):4874-4877.
474 9. Leung KM, *et al.* (2013) *Shewanella oneidensis* MR-1 Bacterial Nanowires Exhibit p-
475 Type, Tunable Electronic Behavior. *Nano Lett.* 13(6):2407-2411.
476 10. Bond DR & Lovley DR (2003) Electricity production by *Geobacter sulfurreducens*
477 attached to electrodes. *Appl. Environ. Microbiol.* 69(3):1548-1555.
478 11. Gregory KB, Bond DR, & Lovley DR (2004) Graphite electrodes as electron donors
479 for anaerobic respiration. *Environ. Microbiol.* 6(6):596-604.
480 12. Marsili E, *et al.* (2008) *Shewanella* Secretes flavins that mediate extracellular electron
481 transfer. *Proc. Natl. Acad. Sci. USA* 105(10):3968-3973.
482 13. Jiang J & Kappler A (2008) Kinetics of microbial and chemical reduction of humic
483 substances: Implications for electron shuttling. *Environ. Sci. Technol.* 42(10):3563-
484 3569.
485 14. Kotloski NJ & Gralnick JA (2013) Flavin Electron Shuttles Dominate Extracellular
486 Electron Transfer by *Shewanella oneidensis*. *Mbio* 4(1): e00553-12.
487 15. Okamoto A, Hashimoto K, Nealson KH, & Nakamura R (2013) Rate enhancement of

bacterial extracellular electron transport involves bound flavin semiquinones. *Proc. Natl. Acad. Sci. USA* 110(19):7856-7861.

16. Okamoto A, *et al.* (2014) Uptake of self-secreted flavins as bound cofactors for extracellular electron transfer in *Geobacter* species. *Energy Environ. Sci.* 7(4):1357-1361.

17. Edwards MJ, *et al.* (2015) Redox Linked Flavin Sites in Extracellular Decaheme Proteins Involved in Microbe-Mineral Electron Transfer. *Sci Rep* 5:11677.

18. Xu S, Jangir Y, & El-Naggar MY (2016) Disentangling the roles of free and cytochrome-bound flavins in extracellular electron transport from *Shewanella oneidensis* MR-1. *Electrochim. Acta.* 198:49-55.

19. Draper RD & Ingraham LL (1968) A potentiometric study of the flavin semiquinone equilibrium. *Arch. Biochem. Biophys.* 125(3):802-808.

20. Okamoto A, *et al.* (2014) Cell-secreted Flavins Bound to Membrane Cytochromes Dictate Electron Transfer Reactions to Surfaces with Diverse Charge and pH. *Sci. Rep.* 4: 5628.

21. Liu XW, *et al.* (2013) Phenothiazine Derivative-Accelerated Microbial Extracellular Electron Transfer in Bioelectrochemical System. *Sci. Rep.* 3: 01616.

22. Tokunou Y, Hashimoto K, & Okamoto A (2016) Acceleration of Extracellular Electron Transfer by Alternative Redox-Active Molecules to Riboflavin for Outer-Membrane Cytochrome *c* of *Shewanella oneidensis* MR-1. *J. Phys. Chem. C* 120(29):16168-16173.

23. Xu S, Barrozo A, Tender LM, Krylov AI, & El-Naggar MY (2018) Multiheme Cytochrome Mediated Redox Conduction through *Shewanella oneidensis* MR-1 Cells. *J. Am. Chem. Soc.* 140(32):10085-10089.

24. Xiong YJ, *et al.* (2006) High-affinity binding and direct electron transfer to solid metals by the *Shewanella oneidensis* MR-1 outer membrane *c*-type cytochrome OmcA. *J. Am. Chem. Soc.* 128(43):13978-13979.

25. Firer-Sherwood M, Pulcu GS, & Elliott SJ (2008) Electrochemical interrogations of the Mtr cytochromes from *Shewanella*: opening a potential window. *J. Biol. Inorg. Chem.* 13(6):849-854.

26. Nakamura R, Ishii K, & Hashimoto K (2009) Electronic Absorption Spectra and Redox Properties of *C* Type Cytochromes in Living Microbes. *Angew. Chem. Int. Ed.* 48(9):1606-1608.

27. Hartshorne RS, *et al.* (2009) Characterization of an electron conduit between bacteria and the extracellular environment. *Proc. Natl. Acad. Sci. USA* 106(52):22169-22174.

523 28. Breuer M, Rosso KM, & Blumberger J (2014) Electron flow in multiheme bacterial
524 cytochromes is a balancing act between heme electronic interaction and redox
525 potentials. *Proc. Natl. Acad. Sci. USA* 111(2):611-616.
526 29. Watanabe HC, Yamashita Y, & Ishikita H (2017) Electron transfer pathways in a
527 multiheme cytochrome MtrF. *Proc Natl. Acad. Sci. USA* 114(11):2916-2921.
528 30. Watanabe HC, Yamashita Y, & Ishikita H (2017) Reply to Breuer et al.: Molecular
529 dynamics simulations do not provide functionally relevant values of redox potential in
530 MtrF. *Proc Natl. Acad. Sci. USA* 114(47):E10029-E10030.
531 31. Barrozo A, El-Naggar MY, & Krylov AI (2018) Distinct Electron Conductance
532 Regimes in Bacterial Decaheme Cytochromes. *Angew. Chem. Int. Ed.* 57(23):6805-
533 6809.
534 32. Okamoto A, Nakamura R, & Hashimoto K (2011) In-vivo identification of direct
535 electron transfer from *Shewanella oneidensis* MR-1 to electrodes via outer-membrane
536 OmcA-MtrCAB protein complexes. *Electrochim. Acta*. 56(16):5526-5531.
537 33. Buckel W & Thauer RK (2018) Flavin-Based Electron Bifurcation, Ferredoxin,
538 Flavodoxin, and Anaerobic Respiration With Protons (Ech) or NAD(+) (Rnf) as
539 Electron Acceptors: A Historical Review. *Front. Microbiol.* 9:401.
540 34. Lubner CE, *et al.* (2017) Mechanistic insights into energy conservation by flavin-
541 based electron bifurcation. *Nat. Chem. Biol.* 13(6):655-659.
542 35. Light SH, *et al.* (2018) A flavin-based extracellular electron transfer mechanism in
543 diverse Gram-positive bacteria. *Nature* 562(7725):140-144.
544 36. You LX, *et al.* (2018) Flavins mediate extracellular electron transfer in Gram-positive
545 *Bacillus megaterium* strain LLD-1. *Bioelectrochemistry* 119:196-202.
546 37. Clarke TA, *et al.* (2011) Structure of a bacterial cell surface decaheme electron conduit.
547 *Proc. Natl. Acad. Sci. USA* 108(23):9384-9389.
548 38. Wang ZM, *et al.* (2015) Effects of soluble flavin on heterogeneous electron transfer
549 between surface-exposed bacterial cytochromes and iron oxides. *Geochim.*
550 *Cosmochim. Acta* 163:299-310.
551 39. Breuer M, Rosso KM, & Blumberger J (2015) Flavin Binding to the Deca-heme
552 Cytochrome MtrC: Insights from Computational Molecular Simulation. *Biophys. J.*
553 109(12):2614-2624.
554 40. Babanova S, *et al.* (2017) Outer membrane cytochromes/flavin interactions in
555 *Shewanella* spp.-A molecular perspective. *Biointerphases* 12(2):021004.
556 41. Johs A, Shi L, Droubay T, Ankner JF, & Liang L (2010) Characterization of the
557 Decaheme *c*-Type Cytochrome OmcA in Solution and on Hematite Surfaces by Small

Angle X-Ray Scattering and Neutron Reflectometry. *Biophys. J.* 98(12):3035-3043.

42. Tokunou Y, *et al.* (2018) Whole-cell circular dichroism difference spectroscopy reveals an *in vivo*-specific deca-heme conformation in bacterial surface cytochromes. *Chem. Commun.* 54(99):13933-13936.

43. Yu SS, Chen JJ, Liu XY, & Yu HQ (2018) Interfacial Electron Transfer from the Outer Membrane Cytochrome OmcA to Graphene Oxide in a Microbial Fuel Cell: Spectral and Electrochemical Insights. *ACS Energy Lett.* 3(10):2449-2456.

44. Tokunou Y & Okamoto A (2019) Geometrical Changes in the Hemes of Bacterial Surface *c*-Type Cytochromes Reveal Flexibility in Their Binding Affinity with Minerals. *Langmuir* 35(23):7529-7537

45. Grattieri M, Rhodes Z, Hickey DP, Beaver K, & Minteer SD (2019) Understanding Biophotocurrent Generation in Photosynthetic Purple Bacteria. *ACS Catal.* 9(2):867-873.

46. Kirchhofer ND, Rengert ZD, Dahlquist FW, Nguyen TQ, & Bazan GC (2017) A Ferrocene-Based Conjugated Oligoelectrolyte Catalyzes Bacterial Electrode Respiration. *Chem* 2(2):240-257.

47. Okamoto A, Tokunou Y, Shafeer K, & Hashimoto K (2017) Proton Transport in the Outer-Membrane Flavocytochrome Complex Limits the Rate of Extracellular Electron Transport. *Angew. Chem. Int. Ed.* 56(31):9082-9086.

48. Rifkin SC & Evans DH (1976) Analytical Evaluation of Differential Pulse Voltammetry at Stationary Electrodes Using Computer-Based Instrumentation. *Anal. Chem.* 48(14):2174-2180.

49. Bard AJ, Faulkner LR, Leddy J, & Zoski CG (1980) Electrochemical methods: fundamentals and applications (John Wiley & Sons, Inc., New York).

50. Burton GW, Joyce A, & Ingold KU (1983) Is Vitamin-E the Only Lipid-Soluble, Chain-Breaking Antioxidant in Human-Blood Plasma and Erythrocyte-Membranes. *Arch. Biochem. Biophys.* 221(1):281-290.

51. Ludwig ML, *et al.* (1997) Control of oxidation-reduction potentials in flavodoxin from *Clostridium beijerinckii*: The role of conformation changes. *Biochemistry* 36(6):1259-1280.

52. Ishikita H (2007) Influence of the protein environment on the redox potentials of flavodoxins from *Clostridium beijerinckii*. *J. Biol. Chem.* 282(35):25240-25246.

53. Corrado ME, Zanetti G, & Mayhew SG (1996) The redox potentials of flavodoxin from *Desulfovibrio vulgaris* and ferredoxin-NADP(+) reductase from *Spinacia oleracea* and their complexes. *Biochem. Soc. Trans.* 24(1):28-28.

593 54. Segal HM, Spatzal T, Hill MG, Udit AK, & Rees DC (2017) Electrochemical and
594 structural characterization of *Azotobacter vinelandii* flavodoxin II. *Protein Sci.*
595 26(10):1984-1993.
596 55. Iyanagi T (2019) Molecular mechanism of metabolic NAD(P)H-dependent electron-
597 transfer systems: The role of redox cofactors. *Biochim. Biophys. Acta* 1860(3):233-258.
598 56. Hartshorne RS, *et al.* (2007) Characterization of *Shewanella oneidensis* MtrC: a cell-
599 surface decaheme cytochrome involved in respiratory electron transport to
600 extracellular electron acceptors. *J. Biol. Inorg. Chem.* 12(7):1083-1094.
601 57. Schmidt am Busch M & Knapp EW (2004) Accurate pK(a) determination for a
602 heterogeneous group of organic molecules. *Chemphyschem* 5(10):1513-1522.
603 58. Matsui T, Baba T, Kamiya K, & Shigeta Y (2012) An accurate density functional
604 theory based estimation of pK_a values of polar residues combined with experimental
605 data: from amino acids to minimal proteins. *Phys. Chem. Chem. Phys.* 14(12):4181-
606 4187.
607 59. Wu YD, Liu TX, Li XM, & Li FB (2014) Exogenous Electron Shuttle-Mediated
608 Extracellular Electron Transfer of *Shewanella putrefaciens* 200: Electrochemical
609 Parameters and Thermodynamics. *Environ. Sci. Technol.* 48(16):9306-9314.
610 60. Tokunou Y, Hashimoto K, & Okamoto A (2018) Electrochemical Detection of
611 Deuterium Kinetic Isotope Effect on Extracellular Electron Transport in *Shewanella*
612 *oneidensis* MR-1. *J. Vis. Exp.* (134):57584.
613 61. Fourmond V, *et al.* (2009) SOAS: A free program to analyze electrochemical data and
614 other one-dimensional signals. *Bioelectrochemistry* 76(1-2):141-147.
615 62. Schowen KB & Schowen RL (1982) Solvent Isotope Effects on Enzyme-Systems.
616 *Method. Enzymol.* 87:551-606.
617 63. Elrod JP, Hogg JL, Quinn DM, Venkatasubban KS, & Schowen RL (1980) Protonic
618 Reorganization and Substrate Structure in Catalysis by Serine Proteases. *J. Am. Chem.*
619 *Soc.* 102(11):3917-3922.
620 64. Reece SY & Nocera DG (2009) Proton-Coupled Electron Transfer in Biology: Results
621 from Synergistic Studies in Natural and Model Systems. *Annu. Rev. Biochem.* 78:673-
622 699.
623 65. Jenson DL & Barry BA (2009) Proton-Coupled Electron Transfer in Photosystem II:
624 Proton Inventory of a Redox Active Tyrosine. *J. Am. Chem. Soc.* 131(30):10567-
625 10573.
626 66. Tokunou Y, Hashimoto K, & Okamoto A (2015) Extracellular Electron Transport
627 Scarcely Accumulates Proton Motive Force in *Shewanella oneidensis* MR-1. *Bull.*

Chem. Soc. Jpn. 88(5):690-692.

67. Bucking C, Popp F, Kerzenmacher S, & Gescher J (2010) Involvement and specificity of *Shewanella oneidensis* outer membrane cytochromes in the reduction of soluble and solid-phase terminal electron acceptors. *FEMS Microbiol. Lett* 306(2):144-151.

68. Jaguar v (2008): Schroinger, LLC, New York, NY.

69. Bashford D & Gerwert K (1992) Electrostatic calculations of the pK_a values of ionizable groups in bacteriorhodopsin. *J. Mol. Biol.* 224(2):473-486.

70. Besler BH, Merz JKM, & Kollman PA (1990) Atomic charges derived from semiempirical methods. *J. Comp. Chem.* 11(4):431-439.

71. Bayly CI, Cieplak P, Cornell WD, & Kollman PA (1993) A well-behaved electrostatic potential based method using charge restraints for deriving atomic charges: the RESP model. *J. Phys. Chem.* 97:10269-10280.

72. Breneman CM & Wiberg KB (1990) Determining atom-centered monopoles from molecular electrostatic potentials. The need for high sampling density in formamide conformational analysis. *J. Comput. Chem.* 11(3):361-373.

73. Lide DR (2001) Handbook of chemistry and physics (Chemical Rubber Publishing, Cleveland).

Figure legends

Fig. 1. (A) Chemical structures of the redox molecules used in the present study. N5 in the isoalloxazine ring is circled in the chemical structure of flavin. Methylene blue (MB), toluidine blue (TB), new methylene blue (NMB), thionine (TN), resorufin (RS), and 1,9-dimethyl-methylene blue (DMMB) have N5, while anthraquinone-1-sulfonate (α-AQS), anthraquinone-1,5-disulfonate (AQDS), 2-methyl-1,4-naphthoquinone (MNQ), and 2-hydroxy-1,4-naphthoquinone (HNQ) lack it. (B) Maximum catalytic current of microbial lactate oxidation in *S. oneidensis* MR-1 (I_c) after 10 h measurement in the presence of each molecule shown in (A). I_c in the presence of flavin, flavin analogs, and quinones are represented as gray, red, and blue bars, respectively. Concentration of each redox molecule was set to 2.0 μM. Error bars represent mean ± SEM for ≥three individual experiments in separate reactors. (C) I_c vs. MB or α-AQS concentration in the reactor. Blue dotted line represents I_c estimated by Fick's law according to the diffusion kinetics of α-AQS between the cell and the electrode. Error bars represent the mean ± SEM for ≥three individual experiments in separate reactors.

Fig. 2. E_0 of the bound cofactors (riboflavin, MB, TB, NMB, and TN) determined by DPV as a function of bulk solution pH. The slopes for the plots are riboflavin: -13 mV pH^{-1}; MB: -34 mV pH^{-1}; TB: -32 mV pH^{-1}; NMB: -30 mV pH^{-1}; and TN: -21 mV pH^{-1}. Inset: E_0 of Cyts derived from the DPV of riboflavin-bound Cyts. The slope was -47 mV pH^{-1} which is near the reported value for MtrC, a subunit of Cyts (56).

Fig. 3. EET capabilities of *S. oneidensis* MR-1 with each N5 molecule as a function of the E_0 of each cofactor (A) and pK_a(N5) in one-electron reduced form (B). The E_0 for all cofactors bound to Cyts except FMN and riboflavin were determined by differential pulse voltammetry (DPV) (Figs. S3 and S4). The E_0 for FMN and riboflavin were obtained from the literature (15, 20). The pK_a(N5) were calculated using a quantum chemical approach (Figs. S10 and S11). pK_a(N5) of FMN and riboflavin were obtained from the literature (19). Error bars represent the mean ± SEM for ≥three individual experiments. The gray dotted line shows the suppression of the EET capability of DMMB relative to MB. The dashed line is for visual guidance and orientation.

679 **Fig. 4.** Effect of deuterium ion on EET kinetics in the presence of redox molecules.
680 Representative time course for current production in the *S. oneidensis* MR-1 monolayer
681 biofilm in the presence of 2.0 μM TN (A) and MB (B). The arrows indicate the time points of
682 D_2O (solid line) or H_2O (dotted line) addition. Data corresponding to the dotted line were
683 normalized to the data point immediately before D_2O addition in the solid line data. (C) Effect
684 of D_2O addition at subtoxic concentrations (≤ 4% v/v) on i_c in the presence of 2.0 μM MB
685 (circle plots) or TN (triangle plots). Data for 2.0 μM riboflavin (square plots) were obtained
686 from the literature (47) for comparison. Error bars represent the mean ± SEM for ≥three
687 experiments in separate reactors. (D) Kinetic isotope effect (KIE) on the EET per unit
688 concentration of the cofactor-bound Cyts complexes in 4% (v/v) D_2O. Error bars represent
689 mean ± SEM for ≥three experiments in separate reactors. Gray dashed line represents the KIE
690 on EET for 4% (v/v) D_2O in the presence of 100 μM α-AQS reported in ref. (47). Numeric
691 data are indicated above each plot.
692
693 **Fig. 5.** Baseline subtracted differential pulse (DP) voltammograms of the *S. oneidensis* MR-1
694 monolayer biofilm in the presence of 2.0 μM riboflavin (A), TN (B), and MB (C). (i) and (ii)
695 represent the data before and after the addition of 4% (v/v) deuterium oxide, respectively.
696 Black and gray lines are baseline subtracted DP voltammograms and fitted lines, respectively.
697 A fitted line composed of two peaks is represented by red and blue lines. According to (15,
698 20), the blue peak is assigned to the Cyts and the red peak is assigned to a bound cofactor.
699 The oxidative peaks in panel (C) were not able to be deconvoluted by SOAS because they
700 overlapped.
701
702 **Fig. 6.** Schematic representation of the molecular control of respiratory electron outflow in *S.*
703 *oneidensis* MR-1 mediated by flavin, flavin analogs, and quinones.